Peer-reviewed version available at Nanomaterials 2020, 10, 426; doi:10.3390/nano10030426

Covalent Organic Framework-Functionalized Magnetic $CuFe_2O_4$/Ag Nanoparticles for the Reduction of 4-Nitrophenol

Chen Hou[a,*], Dongyan Zhao[a], Wenqiang Chen[a], Hao Li[a], Sufeng Zhang[a,*], Chen Liang[b]

[a] *College of Bioresources Chemical and Materials Engineering, Shaanxi University of Science and Technology, Shaanxi Provincial Key Laboratory of Papermaking Technology and Specialty Paper Development, Key Laboratory of Paper Based Functional Materials of China National Light Industry, National Demonstration Center for Experimental Light Chemistry Engineering Education, Xi'an 710021, China*

[b] *Key Laboratory of Clean Pulp & Papermaking and Pollution Control of Guangxi Province, Guangxi University, Nanning 543003, China*

Abstract In this work, magnetic $CuFe_2O_4$/Ag nanoparticles activated by porous covalent organic frameworks (COF) was fabricated to evaluate the heterogenous reduction of 4-nitrophenol (4-NP). The core-shell $CuFe_2O_4$/Ag@COF was successfully prepared by polydopamine reduction of silver ions on $CuFe_2O_4$ nanoparticles, followed by COF layer condensation. With integrating the intrinsic characteristics of the magnetic $CuFe_2O_4$/Ag core and COF layer, the obtained nanocomposite exhibited features of high specific surface area (464.21 m^2 g^{-1}), ordered mesoporous structure, strong environment stability, as well as fast magnetic response. Accordingly, the $CuFe_2O_4$/Ag@COF catalyst showed good affinity towards 4-NP via π-π stacking interactions and possessed enhanced catalytic activity compared with $CuFe_2O_4$/Ag and $CuFe_2O_4$@COF. The pseudo-first-order rate constant of $CuFe_2O_4$/Ag@COF (0.77 min^{-1}) is 3 and 5 times higher than $CuFe_2O_4$/Ag and $CuFe_2O_4$@COF, respectively. The characteristics of bi-catalytic $CuFe_2O_4$/Ag and the porous COF shell of $CuFe_2O_4$/Ag@COF made a contribution to improve the activity of 4-NP reduction. The present work demonstrated a facile strategy to fabricate COF activated nano-catalysts with enhanced performance in the fields of nitrophenolic

wastewater treatment.

Keywords: Magnetic covalent organic frameworks, nanocomposite, core-shell, p-nitrophenol, reduction

1. Introduction

Nitrophenols are mutagenic and refractory aromatic pollutants commonly found in various industrial and agricultural wastewater. Among the three isomeric nitrophenols, 4-nitrophenol (4-NP) is more detrimental to pose a threat to both environment and the public[1]. Generally, two conventional clean up techniques are used for the removal of 4-NP: (1) permanent removal of target contaminats, and (2) conversion into less or no toxic forms. Technique related to the later pattern would be desirable because of the production of *p*-animophenol (4-AP), which is an important intermediate in the productions of pharmaceuticals, dyes, pigments and pesticides[2-4]. Therefore, high efficient and recycled catalysts have been desired for 4-NP reduction.

Catalytic reduction using noble metals as catalysts have been widely employed for 4-NP reduction due to the high surface areas and the exposed active atoms. However, due to the high surface free energy, noble metals tend to agglomerate together, thus leading to obvious decrease of the catalytic activities [5]. To improve the catalytic activity and stability, it would be feasible to immobilize noble metals on a matrix, especially another catalytic component, which would reduce its aggregation as well as improve the catalytic performances in contrast with monometallic counterparts [6, 7].

Magnetic $CuFe_2O_4$ nanoparticles have been used in several water treatment applications due to their desirable stability, easy separation and remarkable

catalysis[8,9]. Thus, instead of single-component metals, noble metal@$CuFe_2O_4$ catalyst would reduce the aggregation of noble metal nanoparticles and maximize the synergistic effects of the bi-catalyst [10,11]. However, because of inter-particle aggregation and non-porous structure, noble metal@$CuFe_2O_4$ nanoparticles still meet sorts of disadvantages such as a limited stability and low surface area. Hence, active noble metal@$CuFe_2O_4$ nanoparticles dispersed on porous solid supports are gaining increasing interests for more effective and versatile catalysis.

Covalent organic frameworks (COF) are an emerging type of most studied porous materials due to the excellent properties and broad applications [12-15]. In comparison with their materials similar to metal organic frameworks (MOF), robust covalent bonds on COF made it overcomes the problems of water and moisture instability [16,17]. The fascinating features such as low density, high and regular porosity, tunable pore size[18,19], rendering them promising candidates in diverse applications in catalysis, gas storage, adsorption, optoelectricity and chemical sensors[20-24]. Recently, some researches have reported that COF can heterogeneously nucleate and grow on the surface of different matrix to construct core-shell structure composite materials (graphene, carbon nanotubes, Fe_3O_4 and alumina, etc.) [25-28]. Incorporation of the merits of COF and nanosized components for core-shell structure nanocomposites synthesis, the aggregation of nanosized cores can be effectively impeded while allowing facile surface modification. Therefore, based on the feasibly tuned properties by the in-built covalent bond architecture, it can be anticipated that COF can be used as more suitable scaffolds than other kinds of

porous materials for fabricating core-shell structured noble metal@$CuFe_2O_4$ nanocomposite.

Herein, a facile synthesis strategy of core-shell structure nanocomposite was developed to integrate magnetic $CuFe_2O_4$/Ag nanoparticles and porous COF for 4-NP reduction. Due to the outstanding stability and chemical robustness[29], TAPB-DMTP (refers to 1,3,5-tris(4-aminophenyl)benzene and 2,5-dimethoxyterephaldehyde, respectively) was utilized as the COF shell material coated on the surface of $CuFe_2O_4$/Ag nanoparticles via PVP assisted encapsulation strategy[30]. Meanwhile, the unique π-π electron structure of COF and strong magnetic property of magnetic $CuFe_2O_4$/Ag@COF composites can provide both affinity sites and the adsorption forces for reaction targets, as well as facilitate the rapid and easy separation. In addition, the high surface area of the TAPB-DMTP coating ensures high loading capacity of the reaction substrates. Accordingly, the as-prepared porous $CuFe_2O_4$/Ag@COF nanocomposite exhibited high surface area, large number of affinity sites and strong magnetic property owing to the combination of the merits of $CuFe_2O_4$/Ag and TAPB-DMTP. By virtue of the unique features, $CuFe_2O_4$/Ag@COF acted as the recyclable catalyst for 4-NP reduction by $NaBH_4$ and shown enhanced catalytic activities and stability.

2. Experimental

2.1 Materials

1,3,5-tris(4-aminophenyl)benzene (TAPB), 2,5-dimethoxyterephaldehyde (DMPT) and dopamine hydrochloride (DA·HCl), Polyethylene glycol (PEG-6000) and

polyvinylpyrrolidone (PVP, Mw=5500) were purchased from Aladdin Co. Ltd (China). Cupric chloride anhydrous ($CuCl_2$), ferric chloride hexahydrate ($FeCl_3 \cdot 6H_2O$), ammonium acetate (NH_4Ac), ethylene glycol (EG), silver nitrate ($AgNO_3$), $NaCH_2COOH$ (NaAc), CH_3COOH (HAc), 4-nitrophenol (4-NP), sodium borohydride ($NaBH_4$), and other chemicals and reagents were purchased from Sinopharm Chemical Reagent Co. Ltd (China).

2.2 Measurements

Sample morphologies were characterized by field emission scanning electron microscopy (SEM, Hitachi S-4800) and transmission electron microscopy (TEM, TECNAI G^2 TF20). Fourier transform infrared (FTIR, Bruker VERTEX 70, Germany) spectra were obtained with a wavelength range of 4000 to 400 cm^{-1}. Powder X-ray diffraction spectra (XRD, Bruker, D8-Advance) were measured with Cu Kα radiation (λ=1.542 Å) in the angle range 5-70° (2θ). The specific surface area and pore size distribution were calculated by the Brunauer-Emmett-Teller (BET, ASAP2460, USA) and Barrett-Joyner-Halanda (BJH) methods. Thermogravimetric analysis (TGA) was recorded on a TG apparatus (NETZSCH STA 449F3-1053-M) by heating the sample in the range 30-800 ℃ at a constant rate of 10 ℃ min^{-1} under a N_2 atmosphere. Magnetic hysteresis loops at room temperature were obtained using a vibrating sample magnetometer VSM 7304 (Lakeshore, Columbus, USA). The chemical composition of $CuFe_2O_4$/Ag and $CuFe_2O_4$/Ag@COF were characterized by X-ray photoelectron spectroscopy (XPS, AXIS SUPRA, UK). The absorbance of the reaction solution was determined by UV-Vis spectra (Shimadzu UV-2501 PC

Peer-reviewed version available at Nanomaterials 2020, 10, 426; doi:10.3390/nano10030426

spectrometer).

2.3 Synthesis of $CuFe_2O_4$/Ag nanoparticles

$CuFe_2O_4$ nanoparticles were synthesized according to the reported method [31]. Then Ag nanoparticle was assembled on $CuFe_2O_4$ according to a polydopamine (PDA) assisted reduction process [32]. Typically, 30 mg of $CuFe_2O_4$ nanoparticles were dispersed in 25 ml Tris buffer solution (10 mM, pH=8.5), followed by adding 50 mg of DA·HCl into the mixture and mechanically stirred for 2 h at room temperature. Then the black powder was collected by a magnet, washed with ethanol and deionized water. For the preparation of $CuFe_2O_4$/Ag nanoparticles, silver ammonia solution was firstly prepared by adding ammonia aqueous solution (2 wt%) into 10 $mg \cdot mL^{-1}$ $AgNO_3$ solution the until brown precipitation was just dissolved. Then 50 mg of PDA modified $CuFe_2O_4$ were added to 25 mL silver ammonia solution, and the mixture was mechanically stirred for 6 h at room temperature. The product was collected with a magnet and washed with ethanol and deionized water, then dried under vacuum at 60 °C over night.

2.4 Preparation of core-shell structured $CuFe_2O_4$/Ag@COF nanocomposites

The synthesis of core-shell structured $CuFe_2O_4$/Ag@COF nanocomposites was carried out as modified method[33]. Firstly, $CuFe_2O_4$/Ag nanoparticles were stabilized with PVP. In brief, the $CuFe_2O_4$/Ag nanoparticles (50 mg) were suspended in water (50 ml), and a solution of PVP (25 mg) in water (50 ml) was added dropwise to the above solution under stirring. The mixture was further stirred at room temperature for 12 h, washed three times with methanol, and final dispersed in

methanol (10 mL). Secondly, the PVP-stabilized $CuFe_2O_4$/Ag nanoparticles were sonicated for 30 min under stirring, and 4 mL 1,4-dioxane-butanol (v/v=1/1) containing TAPB (0.03 mmol) and DMTP (0.045 mmol) was added to the suspension. After that, aqueous acetic acid (12 M, 0.15 mL) was slowly appended to the mixture. Then, the reaction was allowed to conduct at room temperature for 2 h. After another aqueous acetic acid (12 M, 0.45 mL) was added to the suspension, the reaction was further stirred at 70 °C for 24 h. The product ($CuFe_2O_4$/Ag@COF) was naturally cooled to room temperature and collected with the help of a magnet. After being washed with tetrahydrofuran and acetone several times, the product was dried in vacuum at 80 °C overnight.

The $CuFe_2O_4$@COF nanocomposite was prepared according to the above method with adding $CuFe_2O_4$ nanoparticles.

2.5 Catalytic reduction of 4-NP

Catalytic activities of the $CuFe_2O_4$/Ag@COF nanocomposite were evaluated by UV-Vis spectroscopy through the reduction of 4-NP to 4-AP at room temperature, using $NaBH_4$ as a reductant. 200 μL of 4-NP solution (5 mM), 0.45 mL of freshly prepared $NaBH_4$ aqueous solution (200 mM), and 2.35 mL deionized water were added into a standard quartz cuvette. And the mixture solution turns from light yellow to bright yellow. Subsequently, 2 mg of $CuFe_2O_4$/Ag@COF was dispersed to the above mixture. Then the intensity of the absorption peak at 400 nm was monitored by UV-Vis spectroscopy as a function of time. The as-prepared $CuFe_2O_4$ nanoparticles, $CuFe_2O_4$/Ag nanoparticles, and $CuFe_2O_4$@COF nanocomposite were also used as the

contrary catalysts under the same conditions. For the catalyst recycling test, the catalyst was collected with an extra magnet after each cycle, and another 4-NP and $NaBH_4$ solution was added for the next catalytic cycle. The UV-Vis absorption of reaction solution was measured at 400 nm.

3. Results and Discussion

3.1 Fabrication and characterization of $CuFe_2O_4$/Ag@COF nanocomposite

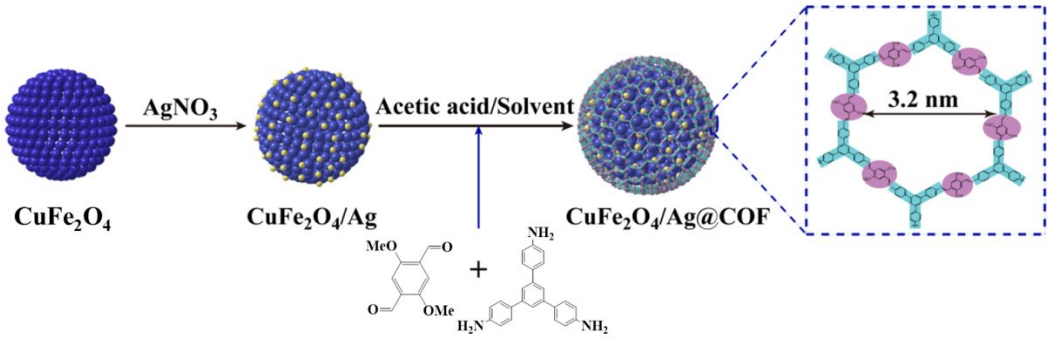

Scheme 1 Schematic representation of the synthesis of core-shell magnetic $CuFe_2O_4$/Ag@COF nanocomposite.

The magnetic $CuFe_2O_4$/Ag@COF was synthesized by using $CuFe_2O_4$/Ag as core, and TAPB-DMTP COF as shell (Scheme 1). $CuFe_2O_4$/Ag was synthesized by depositing Ag on $CuFe_2O_4$ nanoparticles, which was assisted by PDA reduction. This bi-catalyst composed of $CuFe_2O_4$ and *in situ* synthesized Ag nanoparticles would accelerate the 4-NP reduction [34]. The COF shell encapsulation process was assisted by polyvinylpyrrolidone (PVP)-stabilized $CuFe_2O_4$/Ag strategy. Because the amphiphilic PVP has been proved can stabilize the nanoparticles in the reaction solution and enhance the affinity between apolar groups of PVP and organic linkers[30]. Then the TAPB-DMTP was assembled on the surface of $CuFe_2O_4$/Ag based on Schiff-base reaction[33]. The as-prepared nanocomposite has advantages of

Preprints (www.preprints.org) | NOT PEER-REVIEWED | Posted: 4 February 2020 doi:10.20944/preprints202002.0037.v1

Peer-reviewed version available at Nanomaterials 2020, 10, 426; doi:10.3390/nano10030426

large surface area, rapid magnetic response, abundant catalytic sites, which can make sure the high catalytic performance and the catalyst stability towards 4-NP reduction.

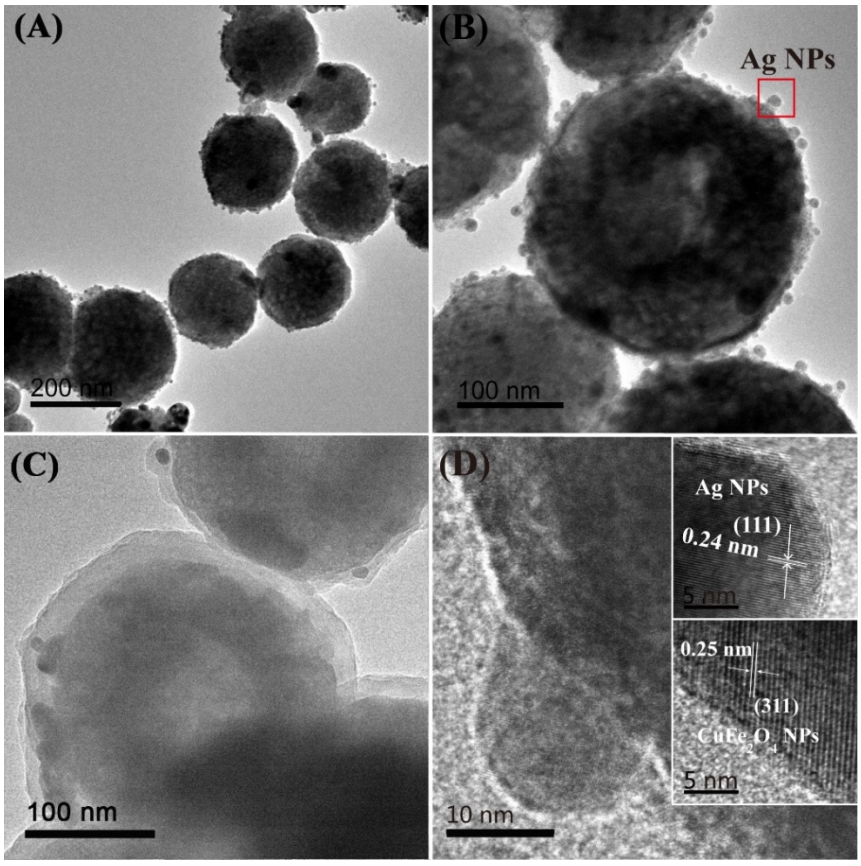

Fig. 1 TEM images of the $CuFe_2O_4$/Ag (A) and (B); $CuFe_2O_4$/Ag@COF (C); and HRTEM image of $CuFe_2O_4$ and Ag (D).

The core-shell structure and morphologies of the as-prepared $CuFe_2O_4$/Ag@COF nanocomposite was verified by Transmission electron microscopy (TEM) and scanning electron microscopy (SEM). Fig. 1A and B revealed that the as-prepared $CuFe_2O_4$/Ag nanoparticles exhibited good monodispersity, and the $CuFe_2O_4$ were spherical in shape with an average diameter of 200 nm. After deposited with Ag nanoparticles, small Ag nanoparticles (~20 nm) were densely and uniformly assembled on the surface of $CuFe_2O_4$. After coated with COF layer, the COF shell (brighter) of TAPB-DMTP networks with a rough surface was formed and the

Preprints (www.preprints.org) | NOT PEER-REVIEWED | Posted: 4 February 2020 doi:10.20944/preprints202002.0037.v1

Peer-reviewed version available at Nanomaterials 2020, 10, 426; doi:10.3390/nano10030426

thickness of *ca.* 30 nm surrounding the $CuFe_2O_4$/Ag core (darker) was clearly observed (Fig. 1C). Meanwhile, at the edges of $CuFe_2O_4$/Ag@COF spheres consisted of domains that contain regular channels along the radial direction (Fig. S1). It is due to the self-assembly of the rod-like crystallites of the COF shell[35], and revealed a highly ordered porous structure of the $CuFe_2O_4$/Ag@COF. Fig. 1D displayed the high-resolution TEM images (HRTEM) and the corresponding fast Fourier transform (FFT) pattern of the $CuFe_2O_4$/Ag@COF nanocomposite. The spacing of the crystallographic plane of the Ag nanoparticles is 0.24 nm, which could be assigned to the (111) crystal planes of face centered cubic (fcc) bulk Ag (0.235 nm). A clear inter planar spacing of the lattice fringes is 0.25 nm, corresponding to the (311) crystal planes of $CuFe_2O_4$ with cubic spinel structure.

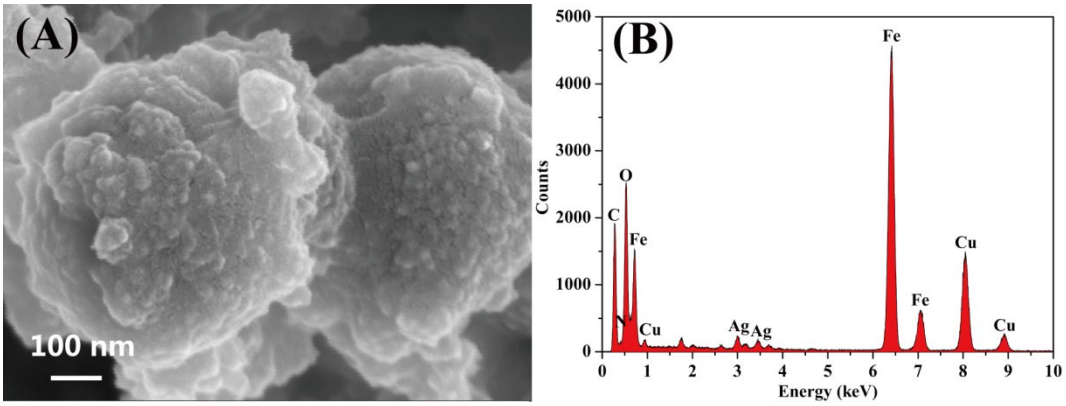

Fig. 2 (A) SEM image of $CuFe_2O_4$/Ag@COF; (B) EDX pattern of $CuFe_2O_4$/Ag@COF.

Furthermore, SEM image of $CuFe_2O_4$/Ag@COF also shown that the nanocomposite consisted of spheres with a rough and coarse surface (Fig. 2A). The obtained nanocomposite is somewhat visible sticky and exhibited convex domains due to the presence of porous TAPB-DMTP. To confirm the elemental composition of the $CuFe_2O_4$/Ag@COF, the EDX elemental mapping confirmed the presence of Cu,

Fe, Ag, C, N, and O element (Fig. 2B).

FTIR was performed to confirm the successful preparation of the $CuFe_2O_4$/Ag@COF nanocomposite (Fig. 3A). In the spectrum of $CuFe_2O_4$/Ag, the absorption broad band at 3430 cm^{-1} represented the stretching mode of -OH groups and another peak at 1620 cm^{-1} corresponded to the bending vibration of H_2O. In the lower zone, peak at 590 cm^{-1} can be related to the vibration of the metal (tetrahedron)-oxygen (M-O), in which the atom M can be copper or iron. Another absorption peak at 428 cm^{-1} was referred to the vibration of octahedral sites of spinel -type oxide[36]. Compared with $CuFe_2O_4$/Ag, similar adsorption bands were observed in the spectrum of the as-prepared $CuFe_2O_4$/Ag@COF nanocomposite. New peaks at 1460 cm^{-1}, 1501 cm^{-1} and 1405 cm^{-1} were assigned to the aromatic C-C ring stretch and methoxy group stretching the of TAPB-DMTP, respectively. Furthermore, the characteristic peaks at 3430 cm^{-1} and 1620 cm^{-1} became strong and sharp due to the existence of N-H bands and C=N vibration of COF coating, validating the successful formation of COF shell via Shiff-base condensation reaction.

The crystallinity of $CuFe_2O_4$/Ag and $CuFe_2O_4$/Ag@COF was investigated by XRD measurements and the result was shown in Fig. 3B. As shown in Fig. 3B, the characteristic diffraction peaks at 2θ = 30.2°, 35.5°, 43.4°, 57.3° and 62.6° corresponding to the (220), (311), (400), (511) and (440) crystal planes of $CuFe_2O_4$ [36]. The pattern at 38.0°, 44.2° and 64.4° can be attributed to the (111), (200) and (220) crystalline planes of the synthesized Ag[37]. After coating of TAPB-DMTP COF, the moderate new peaks at 2θ = 5.60° and 7.4°, and weak peak at 9.7°

Peer-reviewed version available at Nanomaterials 2020, 10, 426; doi:10.3390/nano10030426

belonging to the TAPB-DMTP was observed, which is consistent with that of TAPB-DMTP COF previously reported [29]. These results suggested that the $CuFe_2O_4$/Ag@COF nanocomposite exhibited the crystalline structure feature of magnetic $CuFe_2O_4$/Ag and TAPB-DMTP COF.

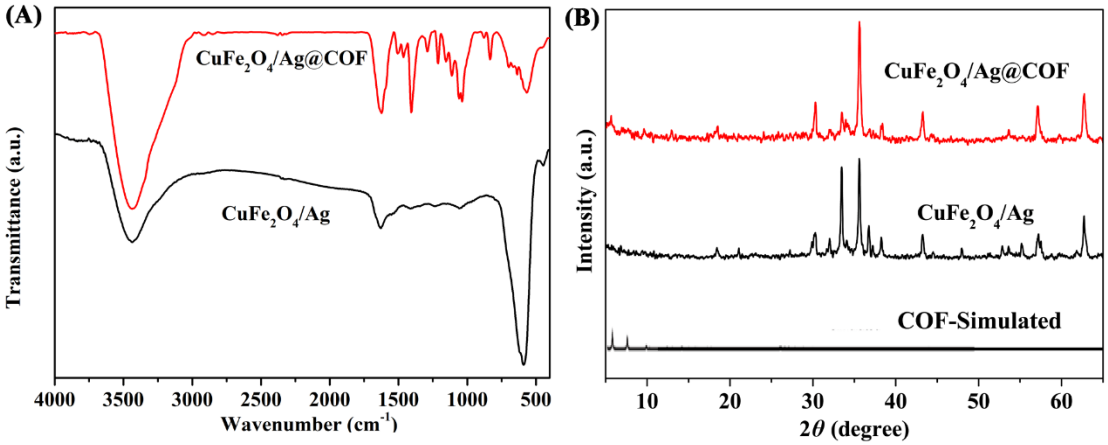

Fig. 3 (A) FTIR spectra of $CuFe_2O_4$/Ag and $CuFe_2O_4$/Ag@COF; (B) XRD patterns of $CuFe_2O_4$/Ag and $CuFe_2O_4$/Ag@COF.

Thermogravimetric analysis (TGA) was further recorded to confirm the content of TAPB-DMTP coatings on the magnetic $CuFe_2O_4$/Ag (Fig. 4A). As for $CuFe_2O_4$/Ag nanoparticles, a distinct weight-loss step of 1.7 wt% up to *ca.* 300 ℃ was observed, which can be attributed to the volatilization of the absorbed water and solvent molecule. Another sharply weight loss profile (5.0 wt%) in the range of 300-400 ℃ was observed due to the decomposition of PDA. Then it remained constant until the temperature rose to 800 ℃, demonstrated a remarkable thermo-stability of $CuFe_2O_4$/Ag. Compared with $CuFe_2O_4$/Ag, the $CuFe_2O_4$/Ag@COF nanocomposite had almost 14 wt% weight losses in the range of 400-700 ℃, implying the decomposition of TAPB-DMTP and further demonstrated the presence of TAPB-DMTP COF shell. Meanwhile, the $CuFe_2O_4$/Ag@COF also exhibited excellent

Preprints (www.preprints.org) | NOT PEER-REVIEWED | Posted: 4 February 2020 doi:10.20944/preprints202002.0037.v1

Peer-reviewed version available at Nanomaterials 2020, 10, 426; doi:10.3390/nano10030426

thermal stability in nitrogen up to 350 ℃.

The pore structure of the $CuFe_2O_4$/Ag@COF was further evaluated by N_2 adsorption-desorption at 77 K (Fig. 4B). The isotherm of $CuFe_2O_4$/Ag presented a typical II characteristics, indicating the obviously nonporous structure of the solid sphere. Compared to $CuFe_2O_4$/Ag, a typical type IV isotherm was observed by $CuFe_2O_4$/Ag@COF, it is indicative of a mesoporous character. From pore size distribution curve (the inset of Fig. 4B), the $CuFe_2O_4$/Ag@COF contained an average pore size of 3.15 nm with narrow sized distribution, which was well in agreement with theoretical value of the bulk COF (3.2 nm)[33]. In addition, the prepared $CuFe_2O_4$/Ag@COF gave an enhanced BET surface area and pore volume of 464.21 $m^2 g^{-1}$ and 0.396 $m^3 g^{-1}$ (38.60 $m^2 g^{-1}$ and 0.0862 $m^3 g^{-1}$ for $CuFe_2O_4$/Ag), respectively (Table S1). The high external surface area with mesoporous structure indicates the superior concentration performance for the substrates, and thus made it possible for $CuFe_2O_4$/Ag@COF to facilitate efficient catalysis reduction of 4-NP.

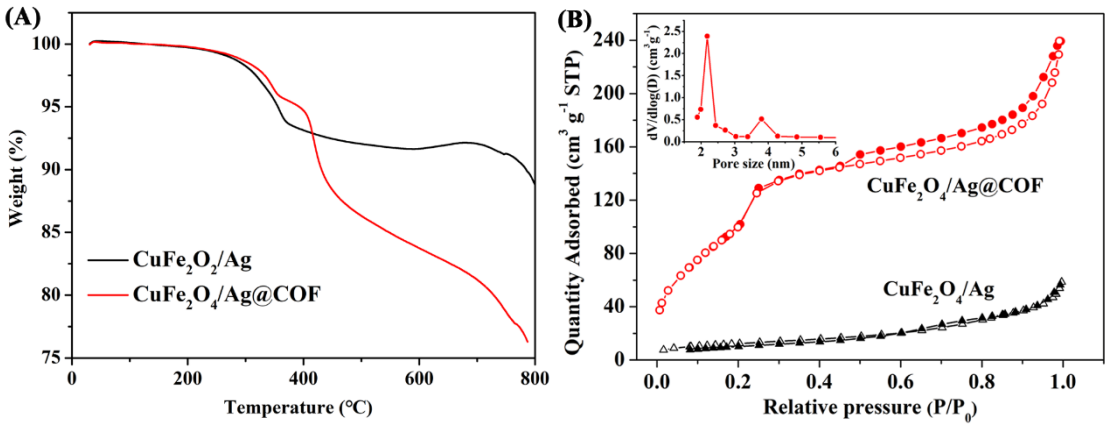

Fig. 4 (A) TGA curves of $CuFe_2O_4$/Ag and $CuFe_2O_4$/Ag@COF (B) N_2 adsorption-desorption isotherms of $CuFe_2O_4$/Ag and $CuFe_2O_4$/Ag@COF (the inset shows pore size distribution of $CuFe_2O_4$/Ag@COF).

Preprints (www.preprints.org) | NOT PEER-REVIEWED | Posted: 4 February 2020 doi:10.20944/preprints202002.0037.v1

Peer-reviewed version available at Nanomaterials 2020, 10, 426; doi:10.3390/nano10030426

The vibrating sample magnetization (VSM) curves of $CuFe_2O_4$/Ag nanoparticle and $CuFe_2O_4$/Ag@COF nanocomposite are shown in Fig. S2. All the obtained materials exhibited superparamagnetic nature due to no obvious coercivity and remanence. After assembled with TAPB-DMTP, the saturation magnetization of $CuFe_2O_4$/Ag@COF decreased from 62.7 emu g^{-1} to 35.1 emu g^{-1}. However, very fast aggregation (about 1 min) of $CuFe_2O_4$/Ag@COF from the homogeneous dispersion was observed with the help of an extra magnet (as shown in the bottom-right inset of Fig. S2).

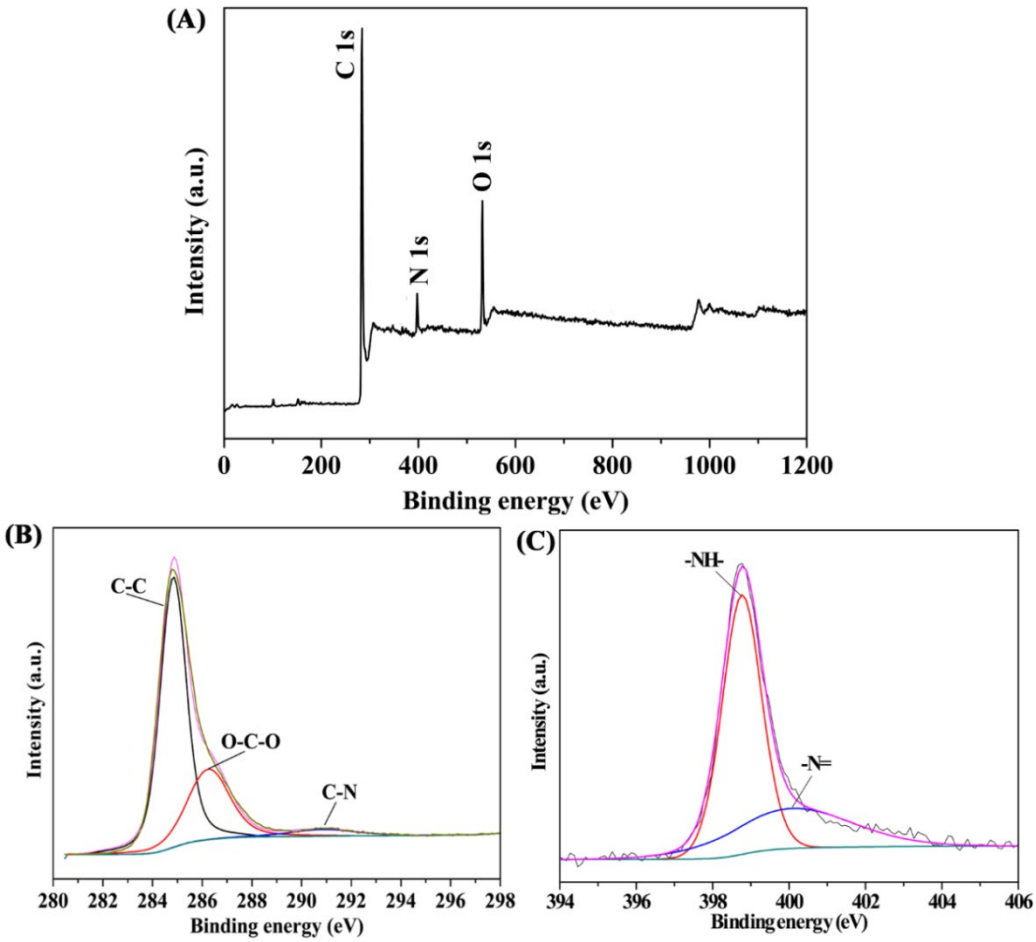

Fig. 5 XPS spectra of $CuFe_2O_4$/Ag@COF: (A) full survey spectrum, (B) C 1s, and (C) N 1s regions.

To further analyze the chemical composition of the magnetic $CuFe_2O_4$/Ag@COF,

X-ray photoelectron spectrometry (XPS) was carried out. In Fig. 5A, the wide scan spectra of the magnetic $CuFe_2O_4$/Ag@COF displayed photoelectron lines at binding energies of 285, 402, and 528 eV, which can be assigned to C 1s, N 1s, and O 1s, respectively. The disappeared Fe, Cu, Ag peaks in the wide scan spectra indicating the inner $CuFe_2O_4$/Ag core was coated with a shell which was thicker than the analysis depth of XPS (~10 nm). The C 1s core-level photoelectron spectrum was split into three peaks located at 284.6, 286.3, and 290.8 eV, respectively (Fig. 5B), which can be attributed to C-C/C=C, C-N, and C=O, respectively. The binding energies observed at Fig. 5C showed the appearance of -NH- and -N= with their characteristic peaks at 398.4 and 400.0 eV. These results confirmed the successful formation of the COF shell.

3.2 Catalytic reduction of 4-NP

The catalytic performance of $CuFe_2O_4$/Ag@COF was tested for reducing 4-NP in the presence of excess $NaBH_4$ in water. The reaction kinetics were monitored by UV-vis absorption spectroscopy of the reaction mixture after adding the catalyst. Notably, the absorption peak of 4-nitrophenol shifts from 319 to 400 nm (the aqueous solution turns from light yellow to bright yellow rapidly) after adding $NaBH_4$ due to the formation of 4-nitrophenolate ions in the alkaline medium.

Fig. 6A and B showed the successive UV-vis spectra of 4-nitrophenolate catalyzed by $CuFe_2O_4$/Ag and $CuFe_2O_4$/Ag@COF in the presence of $NaBH_4$, respectively. The absorption peak at 400 nm was observed to decrease in intensity and new peak at ~300 nm increased along with the reaction time, suggested the reduction of 4-NP to

Peer-reviewed version available at Nanomaterials 2020, 10, 426; doi:10.3390/nano10030426

give 4-AP as the sole product[38]. Fig. 6A shown that the catalytic reduction with $CuFe_2O_4$/Ag nanoparticles could be completed within 11 min. When $CuFe_2O_4$/Ag@COF was used as the catalyst (Fig. 6B), a significant catalytic activity was observed and conversion of 4-NP to 4-AP was finished within 4 min. We can speculate that the momentous activity shown by $CuFe_2O_4$/Ag@COF over $CuFe_2O_4$/Ag own to the porous COF matrix, which provided a large surface area of the encapsulated $CuFe_2O_4$/Ag nanoparticles and high particle number per unit mass for the catalyst. The increased fraction of the substrates at the surface of $CuFe_2O_4$/Ag@COF led to a significantly higher catalytic activity.

Since the concentration of BH_4^- added in the system is in excess compared to the concentration of 4-NP, pseudo-first-order kinetics is expected for the catalytic reaction under this circumstance (Fig. 6C). The pseudo-first-order kinetics can be described as

$$\ln(C_t/C_0) = -kt \quad (1)$$

where C_t is the concentration of 4-NP at time t, C_0 is the initial concentration of 4-NP, and k is the rate constant. From Fig. 6C we can see, all composite samples can catalyze 4-NP reduction but display different activities. Basically, single-catalyst showed lower catalytic activity than the dual-catalyst. For example, $CuFe_2O_4$@COF had a decreased catalytic activity (with the rate constant of 0.15 min^{-1}) and much lower activity for $CuFe_2O_4$ (with the rate constant of 0.08 min^{-1}), respectively, in comparison with that of $CuFe_2O_4$/Ag (0.25 min^{-1}). Moreover, when dual-catalyst was applied, the catalytic performances of the resulting catalysts were inherently influenced by the crystal COF shell. For example, $CuFe_2O_4$/Ag@COF displayed a

higher catalytic activity (with the rate constant of 0.77 min^{-1}) than that of $CuFe_2O_4$/Ag. Specifically, $CuFe_2O_4$/Ag@COF exhibited the highest activity, which was 3, 5 and 10 times higher than that of $CuFe_2O_4$/Ag, $CuFe_2O_4$@COF and $CuFe_2O_4$, respectively. It can be assumed that the sluggish reaction kinetics of the above three kinds of catalysts ($CuFe_2O_4$/Ag, $CuFe_2O_4$@COF and $CuFe_2O_4$) highlighted the utility of dual-catalyst and ordered mesoporous COF shell. This result also showed superior catalytic activity compared to the composite of noble metals (such as Ag, Pd, and Au nanoparticles) embedded in other porous matrix tested under the similar conditions (Table S2).

Additionally, the reusability of $CuFe_2O_4$/Ag@COF was further conducted. With high saturation magnetization, the $CuFe_2O_4$/Ag@COF can be easily separated in a few seconds using an external magnetic field. Fig. 6D displayed the conversion for the reduction of 4-NP in an estimated time span of 4 min. The result displayed excellent reusability of the catalyst for more than 6 catalytic cycles with yields over 95%, indicating excellent reusability and stability towards the as-prepared $CuFe_2O_4$/Ag@COF nanocomposite. The slightly decreased conversions in the later catalysis cycles are presumably caused by the loss of catalyst during the washing process between cycles. The SEM image manifested that the structure of the recycled $CuFe_2O_4$/Ag@COF were preserved and no obvious aggregation was observed further confirmed the excellent stability of the prepared catalyst (Fig. S3). Hence, the prominent catalytic activity and high stability of $CuFe_2O_4$/Ag@COF can be attributed to the highly stable mesoporous architecture (TAPB-DMTP), which held the encapsulated nanoparticles to a high extent and provided docking sites for 4-NP.

Preprints (www.preprints.org) | NOT PEER-REVIEWED | Posted: 4 February 2020 doi:10.20944/preprints202002.0037.v1

Peer-reviewed version available at Nanomaterials 2020, 10, 426; doi:10.3390/nano10030426

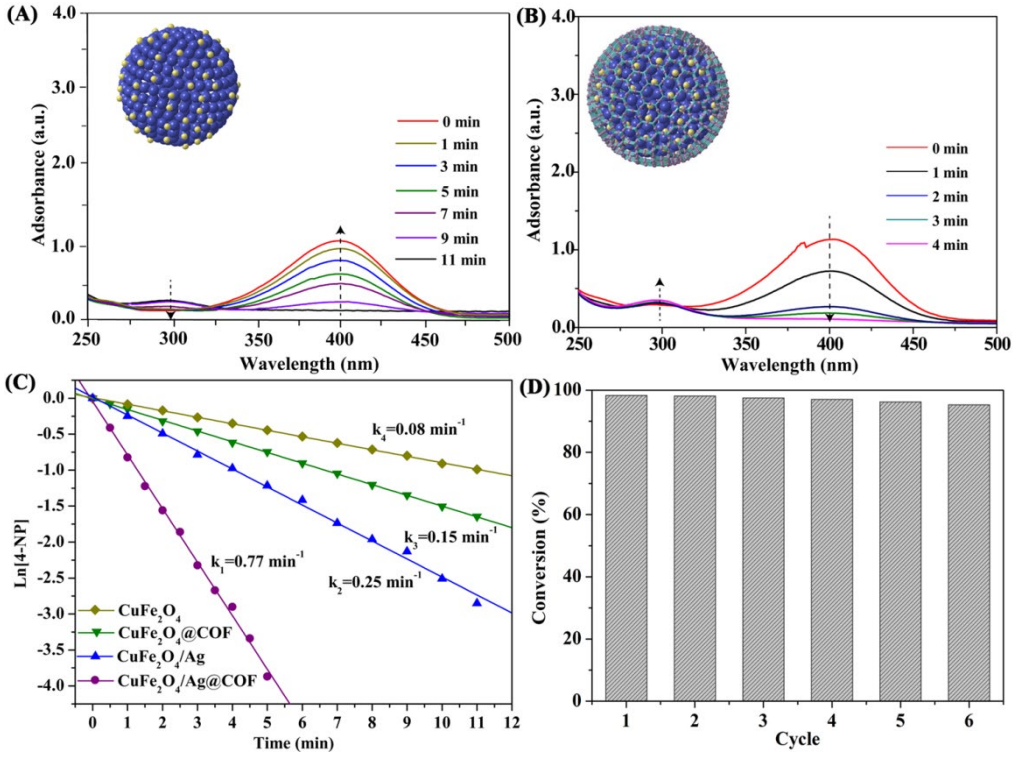

Fig. 6 (A) Typical time-dependent evolution of UV-Vis spectra for the catalytic reduction of 4-NP to 4-AP by $CuFe_2O_4$/Ag; (B) typical time-dependent evolution of UV-Vis spectra for the catalytic reduction of 4-NP to 4-AP by $CuFe_2O_4$/Ag@COF; (C) Relationship of the ln[4-NP] and the reaction time t for the reduction of 4-NP to 4-AP over $CuFe_2O_4$, $CuFe_2O_4$@COF, $CuFe_2O_4$/Ag and $CuFe_2O_4$/Ag@COF; (D) The reusability of $CuFe_2O_4$/Ag@COF for the reduction of 4-NP by $NaBH_4$.

3.3 Plausible mechanisms

Scheme 2 depicts the performance of $CuFe_2O_4$/Ag@COF as catalyst in reducing 4-NP to 4-AP by $NaBH_4$. In aqueous medium, $NaBH_4$ was first diffused through the mesoporous COF shell and adhered onto the surface of $CuFe_2O_4$/Ag, then electrons transferred from $CuFe_2O_4$/Ag to the adsorbed BH_4^- with hydride ions production. Simultaneously, the 4-NP were adsorbed onto the mesoporous COF shell via π-π stacking interactions because 4-NP is π-rich in nature[38]. Subsequently, the hydrogen atom formed from the hydride ions attacked 4-NP molecules to reduce them based on electron transfer to the $CuFe_2O_4$/Ag nanoparticles, forming the product 4-AP[38]. The

Preprints (www.preprints.org) | NOT PEER-REVIEWED | Posted: 4 February 2020 doi:10.20944/preprints202002.0037.v1

Peer-reviewed version available at Nanomaterials 2020, 10, 426; doi:10.3390/nano10030426

surface of dual-catalyst $CuFe_2O_4$/Ag is presumed to play a role in electrically connecting two adsorbates through the surface so that electrons can be transferred from the oxidation site ($NaBH_4$) to the reduction site (4-NP). Such preconcentration of BH_4^- and 4-NP in the COF shell would result a more frequently contact of the inner $CuFe_2O_4$/Ag catalyst with reactants, thereby facilitating the highly efficient catalysis. Moreover, it has been revealed that $CuFe_2O_4$ with 'd^n' (n = 5-9) electronic configuration exhibited better catalytic activity for reduction of nitrophenol[39]. Specifically, both Cu^{2+} and Fe^{3+} ions present in the octahedral sites exposed on the surface of particles, thus the reduction of hydride ions would be accelerated by the enhanced electron transfer boosted by Ag and neighboring $CuFe_2O_4$ nanoparticles (Scheme 2).

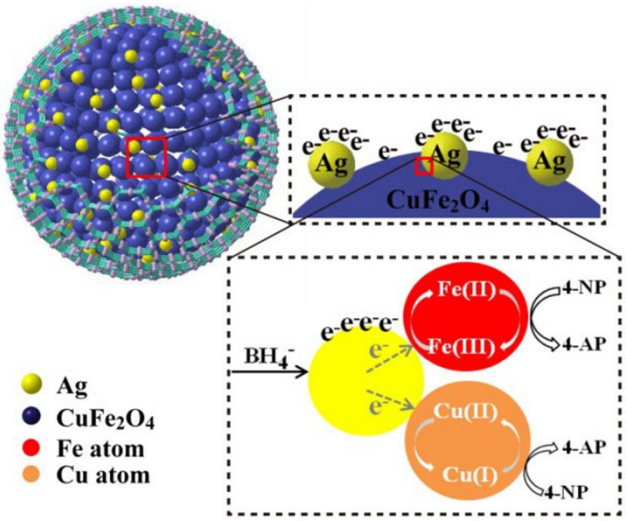

Scheme 2 The mechanism of the reduction of 4-NP to 4-AP by $NaBH_4$ in the presence of $CuFe_2O_4$/Ag@COF.

4. Conclusion

In summary, we have presented a facile and efficient strategy to construct core-shell magnetic $CuFe_2O_4$/Ag@COF nanocomposite. The obtained nanocomposite not only

retained its high crystallinity, large surface area and thermal stability of COF shell, but held high catalytic properties and strong magnetic effect of magnetic $CuFe_2O_4$/Ag nanoparticles. By virtue of these merits, the $CuFe_2O_4$/Ag@COF exhibited enhanced catalytic activity, robust recyclability and stability for the catalytic reduction of 4-NP by $NaBH_4$. Specifically, the apparent reaction rate of $CuFe_2O_4$/Ag@COF was 3 times higher than that by $CuFe_2O_4$/Ag, which can be ascribed to the enhanced $CuFe_2O_4$/Ag dispersion and the strengthened interfacial interaction. Moreover, the magnetic $CuFe_2O_4$/Ag@COF can be easily recycled by a magnet and exhibited robust reusability for six cycles with minimal loss of catalytic activity but held its structural integrity. Encouraged by the effective catalysis of 4-NP with this nanocomposite, it can be expected that rational design of the promising catalytic material with magnetic platforms and tunable porous COF shell will be developed and applied for many redox-active environmental contaminants.

Author Contributions: Conceptualization, C.H. and D.Z.; data curation, D.Z., W.C., and H.L.; formal analysis, D.Z., W.C., and H.L.; methodology, C.H. and D.Z.; software, C.H. and D.Z..; writing—original draft preparation, C.H. and D.Z.; writing—review and editing, C.H.. All authors have read and agreed to the published version of the manuscript.

Acknowledgments: This work was supported by the Guangxi Key Laboratory of Clean Pulping, Papermaking and Pollution Control Opening Fund (KF 201711), and the Open Project Program of National Demonstration Center for Experimental Light Chemistry Engineering Education (Grant No. 2018QGSJ02-09), Shaanxi University of Science & Technology，and the Key Scientific Research Plan of Shaanxi Provincial Education Department (No.17JS016).

Peer-reviewed version available at *Nanomaterials* **2020**, *10*, 426; doi:10.3390/nano10030426

References

1. Agency for Toxic Substances and Disease Registry, Toxicological profile for nitrophenols: 2-nitrophenol, 4-Nitrophenol. U.S. Public Health Service. *Washington D.C* **1992**.
2. Tang, A.; Long, M.; He, Z. Electrodeposition of Sb_2Se_3 on TiO_2 nanotube arrays for catalytic reduction of p-nitrophenol. *Electrochim. Acta* **2014**, *146*, 346-352.
3. Layek, K.; Kantam, M.L.; Shirai, M.; Nishio-Hamane, D.; Sasaki, T.; Maheswaran, H. Gold nanoparticles stabilized on nanocrystalline magnesium oxide as an active catalyst for reduction of nitroarenes in aqueous medium at room temperature. *Green. Chem.* **2012**, *14*, 3164-3174,.
4. Pourjavadi, A.; Safaie, N.; Hosseini, S.H.; Bennett, C. Graphene oxide/poly(imidazole/imidazolium) nanocomposite: An effective support for immobilization of large amounts of Pd nanoparticles. *J. Ind. Eng.* **2016**, *38*, 82-92.
5. Zhang, J.; Zhang, M.; Tang, K.; Verpoort, F.; Sun, T. Polymer-based stimuli-responsive recyclable catalytic systems for organic synthesis. *Small* **2014**, *10*, 32-46.
6. Zhang, S.; Shao, Y.; Liao, H.G.; Liu, J.; Aksay, I.A.; Yin, G.; Lin, Y. Graphene decorated with PtAu alloy nanoparticles: Facile synthesis and promising application for formic acid oxidation. *Chem. Mater*. **2011**, *23*, 1079-1081.
7. Zheng, J.N.; Lv, J.J.; Li, S.S.; Xue, M.W.; Wang, A.J. Feng, J.J. One-pot

synthesis of reduced graphene oxide supported hollow Ag@Pt core-shell nanospheres with enhanced electrocatalytic activity for ethylene glycol oxidation. *J. Mater. Chem. A* **2014**, *2*, 3445-3451.

8. Ren, Y.; Lin, L.; Ma, J.; Feng, J.; Lin, L.Q.; Ren, Y.M. Sulfate radicals induced from peroxymonosulfate by magnetic ferrospinel MFe_2O_4 (M = Co, Cu, Mn, and Zn) as heterogeneous catalysts in the water. *Appl. Catal. B: Environ* **2015**, *165*, 572-578.
9. Du, Y.; Ma, W.; Liu, P.; Zou, B.; Ma, J. Magnetic $CoFe_2O_4$ nanoparticles supported on titanate nanotubes ($CoFe_2O_4$/TNTs) as a novel heterogeneous catalyst for peroxymonosulfate activation and degradation of organic pollutants, *J. Hazard. Mater* **2016**, *308*, 58-66.
10. Zhu, Z.R.; Li, X.Y.; Zhao, Q.D.; Li, Y.H.; Sun, C.Z.; Cao,Y.Q. Photocatalytic performances and activities of Ag-doped $CuFe_2O_4$ nanoparticles. *Mater. Res. Bull* **2013**, *48*, 2927-2932.
11. Zhao, C.H.; Lan, W.Z.; Gong, H.M.; Bai, J.L.; Ramachandran, R.; Liu, S.; Wang, F. Highly sensitive acetone-sensing properties of Pt-decorated $CuFe_2O_4$ nanotubes prepared by electrospinning. *Ceram. Int.* **2018**, *44*, 2856-2863.
12. Cote, A. P.; Benin, A. I.; Ockwig, N. W.; Okeeffe, M.; Matzger, A. J.; Yaghi , O. M. Porous, Crystalline, Covalent Organic Frameworks. *Science* **2005**, *310*, 1166-1170.
13. Waller, P.J.; Gándara, F.; Yaghi, O.M. Chemistry of Covalent Organic Frameworks. *Acc. Chem. Res.* 2015, *48*, 3053-3063.

14. Slater, A.G.; Cooper, A.I. Function-Led Design of New Porous Materials. *Science* **2015**, *348*, 6238-6249.

15. Beuerle F.; Gole B. Covalent Organic Frameworks and Cage Compounds: Design and Applications of Polymeric and Discrete Organic Scaffolds. *Angew Chem. Int. Edit.* **2018**, *57*, 4850-4878.

16. Fei, H.; Cahill, J. F.; Prather, K. A.; Cohen, S. M. Tandem Postsynthetic Metal Ion and Ligand Exchange in Zeolitic Imidazolate Frameworks. *Inorg. Chem.* **2013**, *52*, 4011-4016.

17. Li, H.; Pan, Q.Y.; Ma, Y.C.; Guan, X.Y.; Xue, M.; Fang, Q.R.; Yan, Y.S.; Valtchev, V.; Qiu, S.L. Three-dimensional covalent organic frameworks with dual linkages for bifunctional cascade catalysis. *J. Am. Chem. Soc.* **2016**, *138*, 14783-14788.

18. Dienstmaier, J.F.; Medina, D.D.; Dogru, M.; Knochel, P.; Bein, T.; Heckl, W.M.; Lackinger, M. Isoreticular two-dimensional covalent organic frameworks synthesized by on-surface condensation of diboronic acids. *ACS Nano* **2012**, *6*, 7234-7242.

19. Zhang, F.M.; Sheng, J.L.; Yang, Z.D.; Sun, X.J.; Tang, H.L.; Lu, M.; Dong, H.; Shen, F.C.; Liu, J.; Lan, Y.Q. Rational Design MOF/COF Hybrid Materials for Photocatalytic H_2 Evolution in the Presence of Sacrificial Electron Donors. *Angew Chem. Int. Edit.* **2018**, *130*, 12282-12286.

20. Tylianakis, E.; Klontzasa, E.; Froudakis, G.E. Multi-scale theoretical investigation of hydrogen storage in covalent organic frameworks. *Nanoscale*

2011, *3*, 856-869.

21. Wang, W.; Deng, S.B.; Ren, L.; Li, D.Y.; Wang, W.J.; Vakili, M.; Wang, B.; Huang, J.; Wang, Y.J.; Yu, G. Stable Covalent Organic Frameworks as Efficient Adsorbents for High and Selective Removal of an Aryl-Organophosphorus Flame Retardant from Water. *ACS Appl. Mater. Interfaces* **2018**, *10*, 30265-30272.
22. Dogru, M.; Bein, T. On the road towards electroactive covalent organic frameworks. *Chem. Commun.* **2014**, *50*, 5531-5546.
23. Qian, H.L.; Yang, C.X.; Yan, X.P. Bottom-up synthesis of chiral covalent organic frameworks and their bound capillaries for chiral separation. *Nat. Commun.* **2016**, *7*, 12104-12111.
24. Wang, J.X.; Li, J.; Gao, M.X.; Zhang, X.M. Self-assembling covalent organic frameworks functionalized magnetic graphene hydrophilic biocomposite as an ultrasensitive matrix for N-linked glycopeptide recognition. *Nanoscale* **2017**, *30*, 10750-10756.
25. Yoo, J.T.; Cho, S.J.; Jung, G.Y.; Kim, S.H.; Choi, K.H.; Kim, J.H.; Lee, C.K.; Kwak S.K.; Lee, S.Y. COF-Net on CNT-Net as a Molecularly Designed, Hierarchical Porous Chemical Trap for Polysulfides in Lithium–Sulfur Batteries. *Nano Lett.* **2016**, *16*, 3292-3300.
26. Li, Y.; Yang, C.X.; Yan, X.P. Controllable preparation of core-shell magnetic covalent-organic framework nanospheres for efficient adsorption and removal of bisphenols in aqueous solution. *Chem. Commun.* **2017**, *53*, 2511-2514.

27. Huang, N.; Zhai, L.P.; Coupry, D.E.; Addicoat, M.A.; Okushita, K.; Nishimura, K.; Heine, T.; Jiang, D.L. Multiple-component covalent organic frameworks. *Nat. Commun.* **2016**, *7*, 12325-12335.

28. Xu, H.; Gao, J.; Jiang, D. Stable, Crystalline, Porous, Covalent Organic Frameworks as A Platform for Chiral Organocatalysts. *Nat. Chem.* **2015**, *7*, 905-912.

29. Lu, G.; Li, S.; Guo, Z.; Farha, O.K.; Hauser, B.G.; Qi, X.; Wang, Y.; Wang, X.; Han, S.; Liu, X.; Du, J.S.; Zhang, H.; Zhang, Q.; Chen, X.; Ma, J.; Loo Joachim, S.C.; Wei, W.D.; Yang, Y.; Hupp, J.T.; Huo, F. Imparting Functionality to A Metal-Organic Framework Material by Controlled Nanoparticle Encapsulation. *Nat. Chem.* **2012**, *4*, 310-316.

30. Feng, J.; Su, L.; Ma, Y.H.; Ren, C.L.; Guo, Q.; Chen, X.G. $CuFe_2O_4$ magnetic nanoparticles: A simple and efficient catalyst for the reduction of nitrophenol. *Chem. Eng. J.* **2013**, *221*, 16-24.

31. Sureshkumar, M.; Lee, P.N.; Lee, C.K. Stepwise assembly of multimetallic nanoparticles via self-polymerized polydopamine. *J. Mater. Chem.* **2011**, *21*, 12316-12320.

32. Shi, X.F.; Yao, Y.J.; Xu, Y.L.; Liu, K.; Zhu, G.S.; Chi, L.F.; Lu, G. Imparting Catalytic Activity to a Covalent Organic Framework Material by Nanoparticle Encapsulation. *ACS Appl. Mater. Interfaces* **2017**, *9*, 7481-7488.

33. Lv, Z.S.; Zhu, X.Y.; Meng, H.B.; Feng, J.J.; Wang, A.J. One-pot synthesis of highly branched Pt@Ag core-shell nanoparticles as a recyclable catalyst with

dramatically boosting the catalytic performance for 4-nitrophenol reduction. *J. Colloid and Interf. Sci.* **2019**, *538*, 349-356.

34. Kandambeth, S.; Venkatesh, V.; Shinde, D.B.; Kumari, S.; Halder, A.; Verma, S.; Banerjee, R. Self-Templated Chemically Stable Hollow Spherical Covalent Organic Framework. *Nat. Commun.* **2015**, *6*, 6786.
35. Altincekica, T.G.; Boz, Baykal, A.; Kazan, S.; Topkaya, R.; Toprak, M.S.; Synthesis and characterization of $CuFe_2O_4$ nanorods synthesized by polyol route. *J. Alloy Compd.* **2010**, *493*, 493-498.
36. Zhu, M.; Meng, D.; Wang, C.; Diao, G. Facile fabrication of hierarchically porous $CuFe_2O_4$ nanospheres with enhanced capacitance property. *ACS Appl. Mater. Interfaces* **2013**, *5*, 6030-6037.
37. Zhao, Y.; Tao, C.; Xiao, G.; Wei, G.; Li, L.; Liu, C.; Su, H. Controlled synthesis and photocatalysis of sea urchin-like Fe_3O_4@TiO_2@Ag nanocomposites. *Nanoscale* **2016**, *8*, 5313-5326.
38. Zhang, W.; Lu, G.; Cui, C.; Liu, Y.; Li, S.; Yan, W.; Xing, C.; Chi, Y.R.; Yang, Y.; Huo, F. A Family of Metal-Organic Frameworks Exhibiting Size-Selective Catalysis with Encapsulated Noble-Metal Nanoparticles. *Adv. Mater.* **2014**, *26*, 4056-4060.
39. Feng, J.; Su, L.; Ma, Y.H.; Ren, C.L.; Guo, Q.; Chen, X.G. $CuFe_2O_4$ magnetic nanoparticles: A simple and efficient catalyst for the reduction of nitrophenol, *Chem. Eng. J.* **2013**, *221*, 16-24.